Available online at www.sciencedirect.com
ScienceDirect
Trans. Nonferrous Met. Soc. China 33(2023) 1559−1571
Transactions of Nonferrous Metals Society of China
www.tnmsc.cn

Depression mechanism of $ZnSO_4$ and Na_2CO_3 on talc flotation

Jia-lei LI[1], Yin-yu MA[2], Guang-li LI[3], Zhi-cheng LIU[3],
Shuai NING[1, 4], Bin PEI[1], Zhao-you LANG[3], Rui-zeng LIU[1, 4], Dian-wen LIU[1, 4]

1. Faculty of Land Resources Engineering, Kunming University of Science and Technology, Kunming 650093, China;
2. Xilingol League Shandong Gold Alhada Mining Co., Ltd., Xilingol 026300, China;
3. Yunnan Chihong Zn & Ge Co., Ltd., Qujing 655000, China;
4. Yunnan Key Laboratory of Green Separation and Enrichment of Strategic Mineral Resources, Kunming 650093, China

Received 25 November 2021; accepted 16 June 2022

Abstract: The depression mechanism of a combination of $ZnSO_4$ and Na_2CO_3 on talc during chalcopyrite and molybdenite flotation was investigated in-depth using flotation tests, solution speciation calculations, and various characterization techniques. Flotation tests indicate that the effective depression of talc flotation occurred in the pH range of 7−9. In this pH range, speciation calculations for the mixed solution of $ZnSO_4$ and Na_2CO_3 showed that the $Zn_5(OH)_6(CO_3)_2$ precipitate was the predominant zinc-bearing species, which was further proven by X-ray diffraction and infrared spectroscopy measurements. Zeta potential measurement highlighted that the $Zn_5(OH)_6(CO_3)_2$ precipitate was positively charged while the talc surface was negatively charged in the pH range where talc depression occurred. X-ray photoelectron spectroscopy and field emission scanning electron microscopy confirmed the presence of the zinc-bearing precipitate on the surface of the talc particles treated by the combination of $ZnSO_4$ and Na_2CO_3. These findings suggested that heterocoagulation between the formed $Zn_5(OH)_6(CO_3)_2$ and talc occurred mainly due to the electrostatic attraction, thereby leading to the depression of talc flotation.
Key words: talc; flotation separation; depression; heterocoagulation; electrostatic attraction; $Zn_5(OH)_6(CO_3)_2$

1 Introduction

Talc ($Mg_3Si_4O_{10}(OH)_2$) is commonly present as a gangue mineral in sulfide ores, particularly in Mo, Cu, and Ni sulfide ores, as well as Pt-group metal ores. Talc may be easily reported to these sulfide concentrations because of its inherent floatability, lowering the grade of concentrates [1−3]. Mg-bearing minerals also have a negative impact on the subsequent smelting processes (e.g., raising the liquid temperature and slag viscosity, leading to higher smelting costs) [4−7]. As a result, removing talc from sulfide concentrates is critical in the mineral industry.

The depression of talc in sulfide mineral flotation has piqued interest for decades. In this regard, a class of organic reagents, namely polysaccharides and their derivatives (e.g., carboxymethyl cellulose [7], dextrin/guar gum [8], xanthan gum [9], carrageenan gum [10], and tragacanth gum [11,12]) have been employed for talc depression. However, the industrial applications of these non-toxic and environmentally friendly organic depressants are governed by their high cost [12].

In addition, some inorganic water-soluble salts can also be used for talc depression. When using the

Corresponding author: Rui-zeng LIU, Tel: +86-871-65915598, E-mail: liuruizeng@126.com;
Dian-wen LIU, Tel: +86-871-65915598, E-mail: dianwenliu@kust.edu.cn
DOI: 10.1016/S1003-6326(23)66203-X

metal cations as depressants, FUERSTENAU et al [13] found that talc depression appeared in a pH range between the precipitation pH and the points of zero charges (PZC) of the metal hydroxides. In this pH range, the zeta potential of talc was negative, while that of metal hydroxide was positive, resulting in heterocoagulation between them and then the depression of talc flotation. HUCH and VALLES [14] reported a method of talc-molybdenite separation, which was to use a water-soluble strong acid weak base salt and a water-soluble weak acid strong base salt as depressants. WANG et al [15] investigated the depression mechanism of a combination of zinc sulfate ($ZnSO_4$) and sodium carbonate (Na_2CO_3) on talc flotation, suggesting that the $ZnCO_3$ or $Zn(OH)_2$ precipitated on talc surfaces and then depressed the talc flotation.

The combination of $ZnSO_4$ and Na_2CO_3 can also act as a depressant for sphalerite and arsenopyrite; nevertheless, the mechanisms of depression are seldom investigated. GUAN et al [16] suggested that the depression mechanism of arsenopyrite flotation might be related to the generation of $ZnCO_3$ precipitate, based on the solution chemical speciation calculation performed by WANG et al [15]. However, before gaining a better understanding on the depression mechanism, two key questions must be addressed.

(1) What is the solid product of the mixed solution of $ZnSO_4$ and Na_2CO_3 under flotation-related conditions?

(2) How does the formed solid product interact with talc?

In this study, the flotation behaviors of chalcopyrite, molybdenite, and talc were investigated under different conditions using the combination of $ZnSO_4$ and Na_2CO_3 as talc depressants. To answer the above two questions, various analytical techniques were used to characterize the reaction product and investigate the depression mechanism, including X-ray diffraction (XRD), infrared spectroscopy (IR), zeta potential measurement, field emission scanning electron microscopy coupled with energy dispersive spectroscopy (FESEM-EDS), and X-ray photoelectron spectroscopy (XPS). This work not only offers a better understanding of the depression mechanism of the combination of $ZnSO_4$ and Na_2CO_3 for talc flotation but also provides the important practical guidance.

2 Experimental

2.1 Materials and reagents

Chalcopyrite, molybdenite, and talc samples were obtained from Kunming, China. Lumps of the samples were hand-picked and ground. The 74 to 38 μm size fractions were screened out for flotation, FESEM, and XPS tests. The XRD patterns and chemical analysis results of the prepared samples are shown in Fig. 1 and Table 1, respectively, showing that they were of high purity.

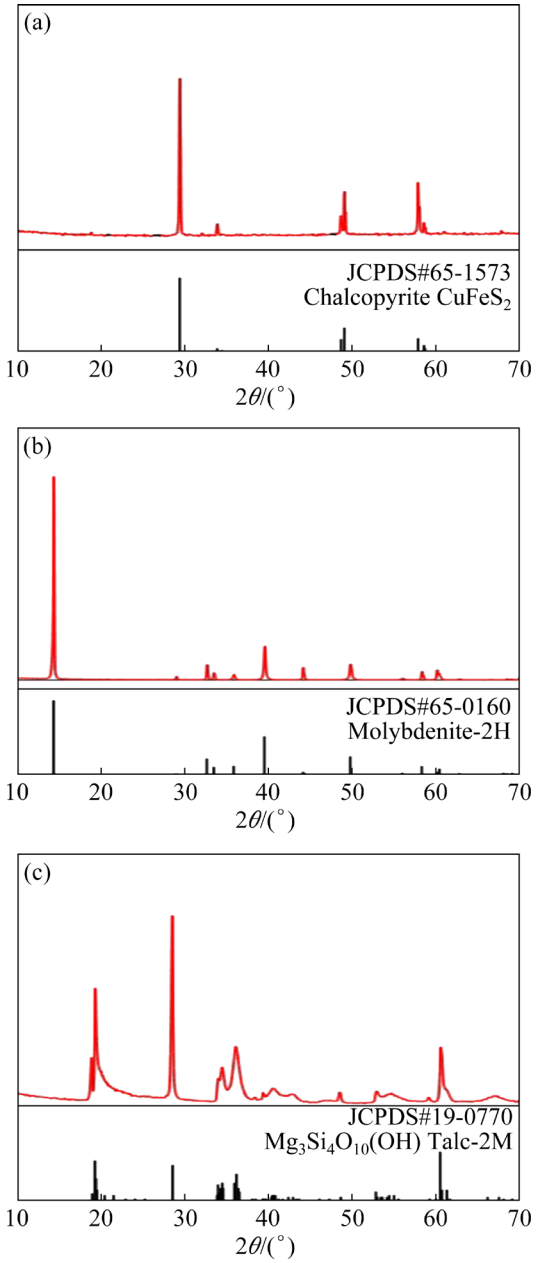

Fig. 1 XRD patterns of chalcopyrite (a), molybdenite (b) and talc (c)

Table 1 Major element content of chalcopyrite, molybdenite and talc samples (wt.%)

Chalcopyrite	Cu	Fe	S	Mg	Si
	31.75	30.84	29.58	0.33	1.83
Molybdenite	Mo	S	Bi	V	Fe
	56.87	39.06	0.26	0.22	0.17
Talc	Si	Mg	O	Fe	Cu
	28.24	18.42	45.72	0.23	0.02

Analytical-grade Na_2CO_3 and $ZnSO_4·7H_2O$ were used as depressants. Analytical-grade NaOH and HCl served as pH modifiers. Industry-grade butyl xanthate (BX) was obtained from Hunan Mingzhu Flotation Reagents Co., Ltd., and acted as a collector in the chalcopyrite−talc separation tests. Analytical-grade kerosene was emulsified with Tween 80, which was used as a collector in the molybdenite−talc separation tests. Analytical-grade methyl isobutyl carbinol (MIBC) was applied as a frother. All analytical-grade reagents were obtained from Macklin Biochemical Co., Ltd (Shanghai, China). All solutions were prepared using deionized water.

2.2 Flotation tests

Batch flotation experiments were carried out in a flotation machine equipped with a 40 mL cell. For the single mineral flotation test, 1.0 g of the mineral sample and a given volume of deionized water were mixed in the cell and then agitated for 1 min. Subsequently, the pH modifiers, the depressants, the collector, and the frother were sequentially injected into the pulp, and each dosing interval was 3 min. After 2 min of flotation, the floated product was gathered, dried and weighed, and the recovery was calculated. After the addition of the depressants and before the addition of the collector and frother, the pulp pH value was measured and reported.

For the artificially mixed minerals flotation test, 1.0 g of talc and 0.5 g of chalcopyrite/molybdenite samples were used. After the above-mentioned flotation operation, the recovery was calculated according to the Cu or Mo grade and the yield of concentrates and tailings.

2.3 Speciation calculations

Speciation calculations for the system Zn^{2+}–CO_3^{2-}–H_2O were conducted by Medusa software to study the reaction of $ZnSO_4$ solution with $NaCO_3$ solution [17,18].

2.4 XRD and IR analyses

XRD and IR analyses were carried out to determine the phase composition of the precipitate produced from the mixed solution of $ZnSO_4$ and Na_2CO_3. Prior to measurements, the sample was prepared as follows: A mixed solution containing 1mmol/L $ZnSO_4$ and 1 mmol/L Na_2CO_3 was stirred for 3 min by a mechanical stirrer. Subsequently, the formed precipitate from the mixed solution was filtered, washed, and dried. XRD measurement was performed using an Ultima IV X-ray diffractometer (Cu K_α radiation, λ=1.5406 Å, scanning speed 2 (°)/min); IR measurement was carried out in a Bruker's Alpha infrared spectrometer with 4 cm^{-1} resolution.

2.5 Zeta potential measurements

The zeta potential was measured using a Malvern Zetasizer Zeta Nano analyzer (Zetasizer-3000 HS). In this test, 0.05 g of talc fines or the formed precipitate obtained in Section 2.4 was dispersed in 40 mL of 1 mmol/L KCl solution. After agitation and pH adjustment by NaOH and HCl, 1 mL of this suspension was sampled and then injected into the sample cell to measure.

2.6 XPS analyses

XPS spectra were obtained using a PHI5000 VersaProbe II instrument (ULVAC-PHI, Japan) with an Al K_α X-ray source. The obtained spectra were calibrated using the C 1s binding energy at 284.8 eV [19,20]. To prepare the XPS sample, 1 g of talc was mixed with 40 mL of a solution containing 1 mmol/L $ZnSO_4$ and 1 mmol/L Na_2CO_3. After treatment for 3 min, the talc particles were filtered, washed, and dried for measurement.

2.7 FESEM-EDS measurements

To observe whether the solid product of the mixed solution of $ZnSO_4$ and Na_2CO_3 precipitated on the talc surfaces, FESEM-EDS measurements were taken using a field emission scanning electron microscope (Gemini 300, Zeiss) equipped with an energy dispersive spectrometer (Oxford X-Max). The FESEM sample preparation was similar to that of the XPS sample. However, just 0.1 g of talc sample was utilized. The talc sample was coated with platinum prior to testing.

3 Results and discussion

3.1 Flotation tests

Figure 2(a) shows the flotation recovery of chalcopyrite and talc as a function of $ZnSO_4$ and Na_2CO_3 concentration. As the concentrations of $ZnSO_4$ and Na_2CO_3 increased, the chalcopyrite recovery slightly decreased, while the talc recovery significantly dropped. Similar results were obtained for the flotation of molybdenite and talc when using emulsified kerosene as a collector (Fig. 2(b)). As can be seen from Figs. 2(a) and (b), talc flotation was effectively depressed, while chalcopyrite and molybdenite maintained good floatability when both concentrations of $ZnSO_4$ and Na_2CO_3 were 1 mmol/L. Figure 2(c) shows the effect of the concentration of $ZnSO_4$ and Na_2CO_3 on the pH of talc pulp. The pH of pulp is in the range of 6.41−7.49 under the conditions depicted in Fig. 2(c). When comparing Figs. 2(a) and (b), it can be seen that the depression performance of the combined depressants in the talc−molybdenite system is lower than that in the talc−chalcopyrite system due to the fact that kerosene can collect talc while xanthate cannot, showing that the talc−molybdenite separation is more difficult.

The effect of pulp pH adjusted by NaOH or HCl on the depression of talc flotation is depicted in Fig. 3(a). Figure 3(a) shows that the effective depression of talc flotation occurred in the pH range of 7−9; however, the depression performance weakened or even disappeared beyond this pH range. Similar results were observed upon adjusting the concentration ratio of Na_2CO_3 to $ZnSO_4$ to adjust the pulp pH (Fig. 3(b)). As the molar concentration ratio of Na_2CO_3 to $ZnSO_4$ increased from 1 to 2, the pH of the pulp increased from 6.88 to 8.63, and the flotation recovery of talc gradually decreased. However, as the ratio continued to increase, the recovery gradually increased; in particular, 84.83% talc recovery was obtained with 3 mmol/L Na_2CO_3.

Figure 4(a) depicts the flotation separation results of chalcopyrite from talc. Without the addition of depressants, the produced concentrate contained 14.6 wt.% Cu and 18.88 wt.% MgO, indicating a 95.52% Cu recovery and a 57.25% MgO recovery. However, when the combination of $ZnSO_4$ and Na_2CO_3 was used, the produced concentrate contained 23.89 wt.% Cu and 10.78 wt.% MgO, representing a 93.77% Cu recovery and a 23.25% MgO recovery. The separation results of molybdenite from talc are shown in Fig. 4(b). In the absence of depressants, the obtained concentrate

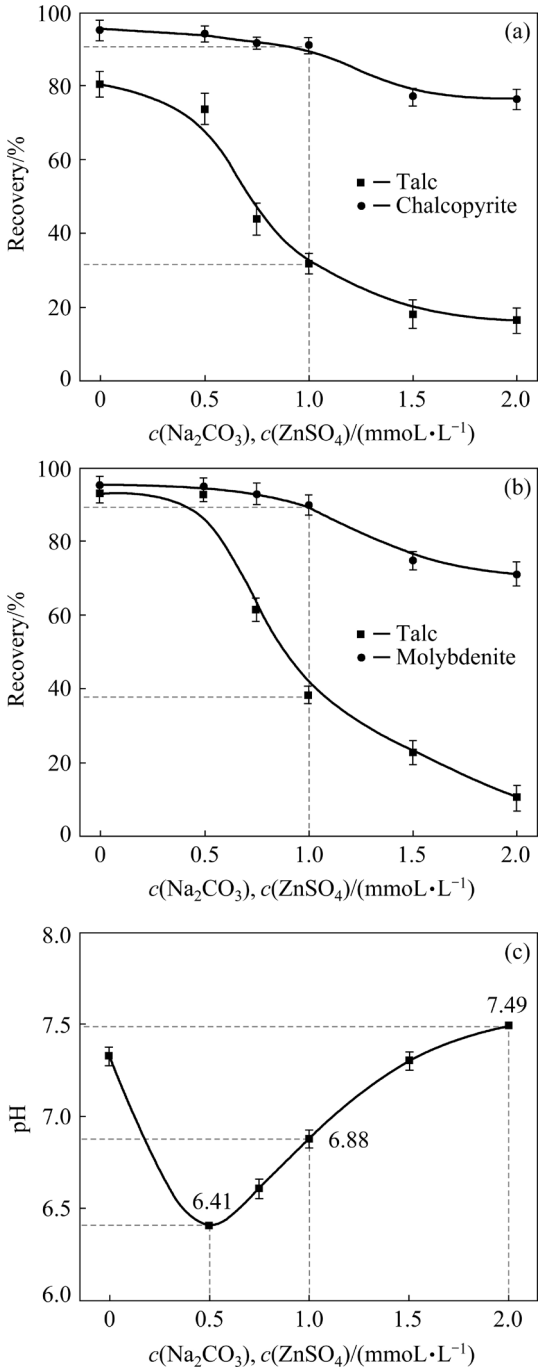

Fig. 2 Flotation recovery of talc and chalcopyrite as function of $ZnSO_4$ and Na_2CO_3 concentration in natural pH (a) (ρ(MIBC)=20 mg/L, ρ(BX)=20 mg/L), flotation recovery of talc and molybdenite as function of $ZnSO_4$ and Na_2CO_3 in natural pH (b) (ρ(MIBC)=20 mg/L, ρ(EK)=20 mg/L), and pulp pH of talc as function of $ZnSO_4$ and Na_2CO_3 concentration (c)

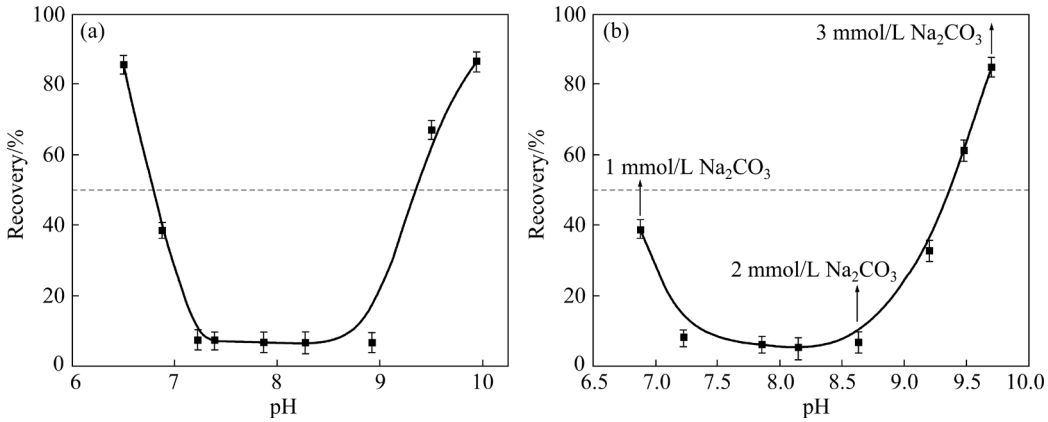

Fig. 3 Talc recovery versus pH adjusted by HCl and NaOH (a) ($c(ZnSO_4)$=1 mmol/L, $c(Na_2CO_3)$=1 mmol/L, ρ(MIBC)=20 mg/L, ρ(EK)=20 mg/L), and by Na_2CO_3 (b) ($c(ZnSO_4)$=1 mmol/L, ρ(MIBC)=20 mg/L, ρ(EK)=20 mg/L)

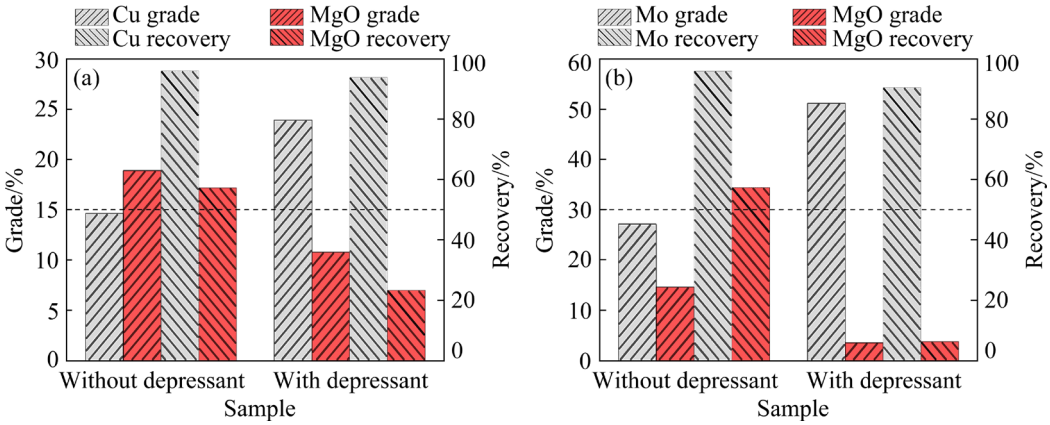

Fig. 4 Flotation separation results of chalcopyrite and talc (a) ($c(ZnSO_4)$=1 mmol/L, $c(Na_2CO_3)$=1 mmol/L, pH=7.25, ρ(MIBC)=20 mg/L, ρ(BX)=20 mg/L), and molybdenite and talc (b) ($c(ZnSO_4)$=2 mmol/L, $c(Na_2CO_3)$=2 mmol/L, pH=7.30, ρ(MIBC)=20 mg/L, ρ(EK)=20 mg/L)

contained 27.1 wt.% Mo and 14.58 wt.% MgO, showing a 95.83% Mo recovery and a 57.31% MgO recovery; however, in the presence of depressants, a concentrate with a grade of 51.1 wt.% Mo and 3.53 wt.% MgO was obtained, suggesting a 90.38% Mo recovery and a 6.21% MgO recovery.

The flotation results show that the combination of $ZnSO_4$ and Na_2CO_3 can offer good depression performance for talc and selectivity towards sulfide minerals such as chalcopyrite and molybdenite.

3.2 Solution chemistry for Zn^{2+}–CO_3^{2-}–H_2O system

Table 2 summarizes the reactions and their equilibrium constants (lg K) for the system of Zn^{2+}–CO_3^{2-}–H_2O included in Medusa Software. Based on Table 2, the equilibrium concentrations and fraction of zinc species of the mixed solution as a function of pH, under different conditions, are calculated and plotted in Fig. 5. The results of the speciation calculation show that zinc can precipitate as $ZnCO_3$, $Zn(OH)_2$, $Zn_5(OH)_6(CO_3)_2$ and ZnO in the system of Zn^{2+}–CO_3^{2-}–H_2O, which depend on the $ZnSO_4$ concentration, Na_2CO_3 concentration and pH.

Figure 5(a) depicts the distribution of species in an aqueous solution containing 1 mmol/L CO_3^{2-} and 1 mmol/L Zn^{2+}. At a given pH, concentration difference among these species in solution can be over one or many orders of magnitude, as seen in the lg[Zn^{2+}]–pH plot. When pH is between 6.67 and 9.64, $Zn_5(OH)_6(CO_3)_2$ precipitate is the main zinc species; however, when pH is below 6.67 and above 9.64, Zn^{2+} and ZnO precipitates become the dominant zinc species, respectively. As the concentration of CO_3^{2-} (2 mmol/L and 3 mmol/L) increased while Zn^{2+} concentration was maintained at 1 mmol/L, the fraction of $ZnCO_{3(s)}$ precipitate

Table 2 Equilibrium constants for reactions of mixed solution of $ZnSO_4$ and Na_2CO_3

Reaction	lg *K*
$2H^+ + CO_3^{2-} = CO_2(g) + H_2O$	18.149
$2H^+ + CO_3^{2-} = H_2CO_3$	16.681
$H^+ + CO_3^{2-} = HCO_3^-$	10.329
$H_2O = H^+ + OH^-$	14.0
$Zn^{2+} + 2CO_3^{2-} = Zn(CO_3)_2^{2-}$	9.63
$Zn^{2+} + 2H_2O = 2H^+ + Zn(OH)_2$	−16.4
$Zn^{2+} + 3H_2O = 3H^+ + Zn(OH)_3^-$	−28.2
$Zn^{2+} + 4H_2O = 4H^+ + Zn(OH)_4^{2-}$	−41.3
$2Zn^{2+} + 6H_2O = 6H^+ + Zn_2(OH)_6^{2-}$	−54.3
$2Zn^{2+} + 2H_2O = H^+ + Zn_2(OH)_3^+$	−9.0
$4Zn^{2+} + 4H_2O = H^+ + Zn_4(OH)_4^{4-}$	−27.0
$Zn^{2+} + CO_3^{2-} = ZnCO_3$	5.3
$Zn^{2+} + CO_3^{2-} + H^+ = ZnHCO_3^+$	12.429
$Zn^{2+} + H_2O = H^+ + ZnOH^+$	−7.5
$Zn^{2+} + 2H_2O = 2H^+ + Zn(OH)_2(s)$	−12.45
$5Zn^{2+} + 2CO_3^{2-} + 6H_2O = 6H^+ + Zn_5(OH)_6(CO_3)_2(s)$	9.7
$Zn^{2+} + CO_3^{2-} = ZnCO_3(s)$	10.0
$Zn^{2+} + 2H_2O = 2H^+ + ZnO(cr)$	−11.2

significantly increased in the pH range of 6−7 (Figs. 5(b) and (c)). However, in the pH range of 7−9, where the effective depression of talc flotation occurred, $Zn_5(OH)_6(CO_3)_2$ precipitate is invariably the main zinc-bearing species.

According to the previous research, under normal circumstances, $Zn_5(OH)_6(CO_3)_2$ is the most common product, whereas $ZnCO_3$ is only generated at acidic pH, high CO_2 partial pressure, or low temperature [21]. According to JAMBOR [22], efforts to synthesize $ZnCO_3$ almost always result in the production of $Zn_5(OH)_6(CO_3)_2$. ALWAN and WILLIAMS [23] reported that the precipitation of $ZnCO_3$ is impossible under normal conditions. Such findings show that the depression of the combination of $ZnSO_4$ and Na_2CO_3 for mineral flotation should be attributed more to $Zn_5(OH)_6(CO_3)_2$ rather than $ZnCO_3$.

3.3 Phase composition determination of produced precipitate

Figure 6 shows the XRD pattern of the precipitate produced from the mixed solution with 1 mmol/L $ZnSO_4$ and 1 mmol/L Na_2CO_3 at pH 7.50. Peaks appearing in the precipitate can be indexed to hydrozincite $Zn_5(OH)_6(CO_3)_2$ (PDF# 19-1458). No impurity peaks were observed, confirming the high purity of the formed $Zn_5(OH)_6(CO_3)_2$. The broad peaks indicate that the formed $Zn_5(OH)_6(CO_3)_2$ precipitate is nanocrystalline [24,25], hinting the formed $Zn_5(OH)_6(CO_3)_2$ precipitate with colloidal size. Figure 7 shows the IR spectrum of the formed precipitate in the range of 2000−400 cm^{-1}, which is in good agreement with the previous IR studies on hydrozincite [21,26−28]. The assignment of several typical bands of the IR spectra to the produced precipitate is summarized in Table 3. The bands at 1511 and 1388 cm^{-1} are attributed to the carbonate v_3 mode (the asymmetric C—O stretching mode). The band at 1109 cm^{-1} is probably due to the carbonate v_1 mode (the symmetric C—O stretching mode). The band at 833 cm^{-1} is attributed to the carbonate v_2 mode (out-of-plane OCO bending mode) and the bands at 740 and 709 cm^{-1} to the carbonate v_4 mode (the asymmetric OCO bending mode). The bands at 1044 and 951 cm^{-1} are attributed to libration of OH^- bonded to zinc ions in hydrozincite.

Using XRD and IR measurements, the phase composition of the produced precipitate under flotation-related circumstances was identified as hydrozincite $Zn_5(OH)_6(CO_3)_2$, which accords with the speciation calculation results.

3.4 Surface charges of talc and produced precipitate

The effect of pH on the zeta potential of talc and precipitate produced from the mixed solution of $ZnSO_4$ and Na_2CO_3 was studied to shed light on the depression mechanism of talc flotation. Since talc is a typical plate-like anisotropic mineral that carries distinct electrical charges on its basal planes and edges, the measured zeta potential should only be considered to be apparent and comparative [1]. As can be seen in Fig. 8, the PZC of the talc sample is at pH 1.5, indicating that the apparent zeta potential of talc is negative at pH above 1.5; moreover, the apparent zeta potential of talc particles becomes more negative as the pH increases. The PZC of the formed $Zn_5(OH)_6(CO_3)_2$ precipitate was observed at pH 9.4, which means that the zeta potential of the formed precipitate is positive at pH below 9.4 and negative at pH above 9.4. In the studied pH range, the zeta potential of the formed $Zn_5(OH)_6(CO_3)_2$ precipitate was ±20 mV.

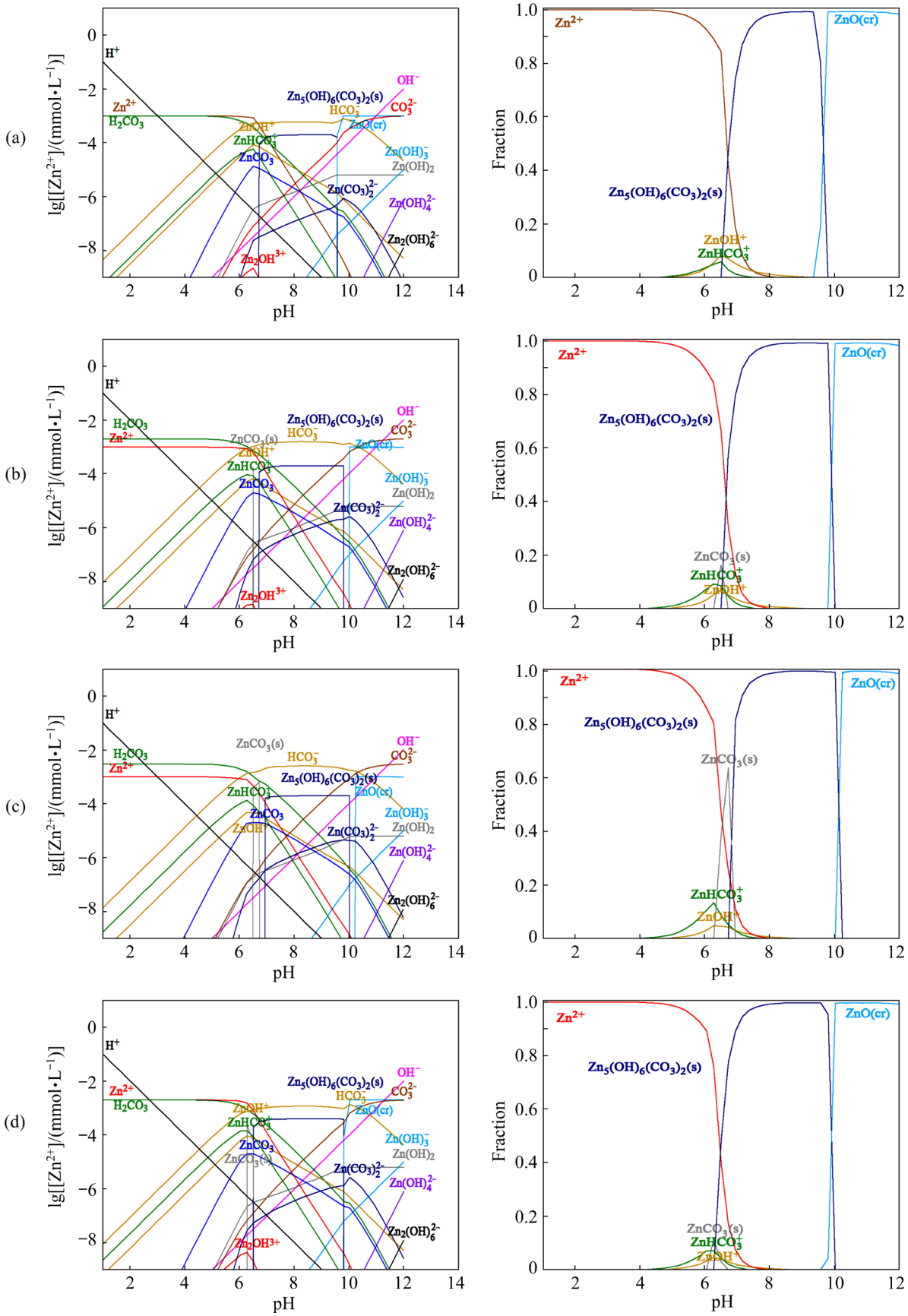

Fig. 5 Equilibrium concentrations (lg$c$[Zn^{2+}]) and fraction of zinc species of mixed solution of $ZnSO_4$ and Na_2CO_3 as function of pH under different conditions: (a) $[CO_3^{2-}]_{TOT}$=1 mmol/L, $[Zn^{2+}]_{TOT}$=1 mmol/L; (b) $[CO_3^{2-}]_{TOT}$=1 mmol/L, $[Zn^{2+}]_{TOT}$=2 mmol/L; (c) $[CO_3^{2-}]_{TOT}$=1 mmol/L, $[Zn^{2+}]_{TOT}$=3 mmol/L; (d) $[CO_3^{2-}]_{TOT}$=2 mmol/L, $[Zn^{2+}]_{TOT}$=2 mmol/L

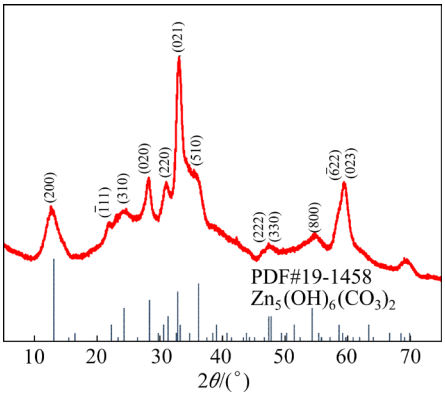

Fig. 6 XRD pattern of precipitate produced from mixed solution with 1 mmol/L $ZnSO_4$ and 1 mmol/L Na_2CO_3 at pH 7.50

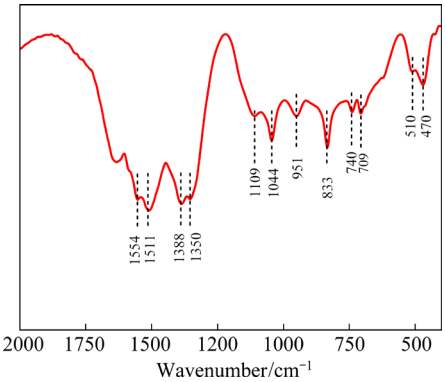

Fig. 7 IR spectrum of precipitate produced from mixed solution with 1 mmol/L $ZnSO_4$ and 1 mmol/L Na_2CO_3 at pH 7.50

Table 3 Results of IR spectra for produced precipitate and references used for identification

Wavenumber/cm^{-1}	Band assignment	Ref.
1511	CO_3 (v_3), component 1	[26]
1388	CO_3 (v_3), component 2	[26]
1109	CO_3 (v_1)	[28]
1044	OH libration	[28]
833	CO_3 (v_2)	[26]
951	OH libration	[28]
740	CO_3 (v_4), component 1	[26]
709	CO_3 (v_4), component 2	[26]

The results of zeta potential measurement revealed that the produced $Zn_5(OH)_6(CO_3)_2$ precipitate is positively charged whereas the talc particle is negatively charged in the pH range of 7−9, where the effective depression of talc flotation occurred.

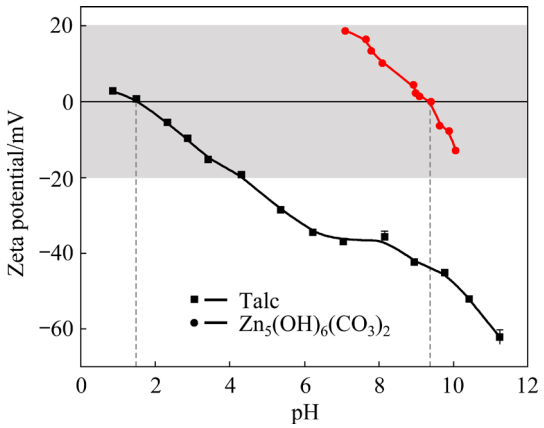

Fig. 8 Zeta potential of talc and formed $Zn_5(OH)_6(CO_3)_2$ precipitate as function of pH

3.5 Surface chemical of talc treated by $ZnSO_4$ and Na_2CO_3

XPS analyses were performed to characterize the surface chemical of talc depressed by the combination of $ZnSO_4$ and Na_2CO_3 on talc flotation. Figure 9(a) presents the survey scan spectra of talc treated with and without the mixed solution of $ZnSO_4$ and Na_2CO_3, where the photoelectron lines or Auger lines for Mg, Si, O, and C stood out. However, no significant difference in the chemical components was observed. As depicted in the inset of Fig. 9(a), both C 1s peaks at 284.80 eV appeared single and symmetric, which was primarily attributable to the adventitious carbon contamination.

The detailed scan results of the Zn 2p region for the talc samples treated with and without the mixed solution of $ZnSO_4$ and Na_2CO_3 are shown in Fig. 9(b). For the untreated sample, only one peak appeared in this region, which was a part of the O KLL Auger lines (Fig. 9(b_1)). For the sample treated with the combined depressants, besides the O KLL Auger peak, Zn 2p peaks emerged, containing a spin-orbit doublet consisting of Zn $2p_{3/2}$ (1022.39 eV) and Zn $2p_{1/2}$ (1045.36 eV). As expected, the doublet has a spin-orbit separation of 22.97 eV and a Zn $2p_{3/2}$-to-Zn $2p_{1/2}$ peak area ratio of 2:1 (Fig. 9(b_2)). High-resolution Zn LMM Auger spectra, which are more sensitive to difference in the chemical state [29], are shown in Figs. 9(c_1, c_2). In the spectrum of the untreated talc sample, no peak was observed. However, for the treated sample, a Zn LMM Auger peak appeared at the kinetic energy of 986.65 eV.

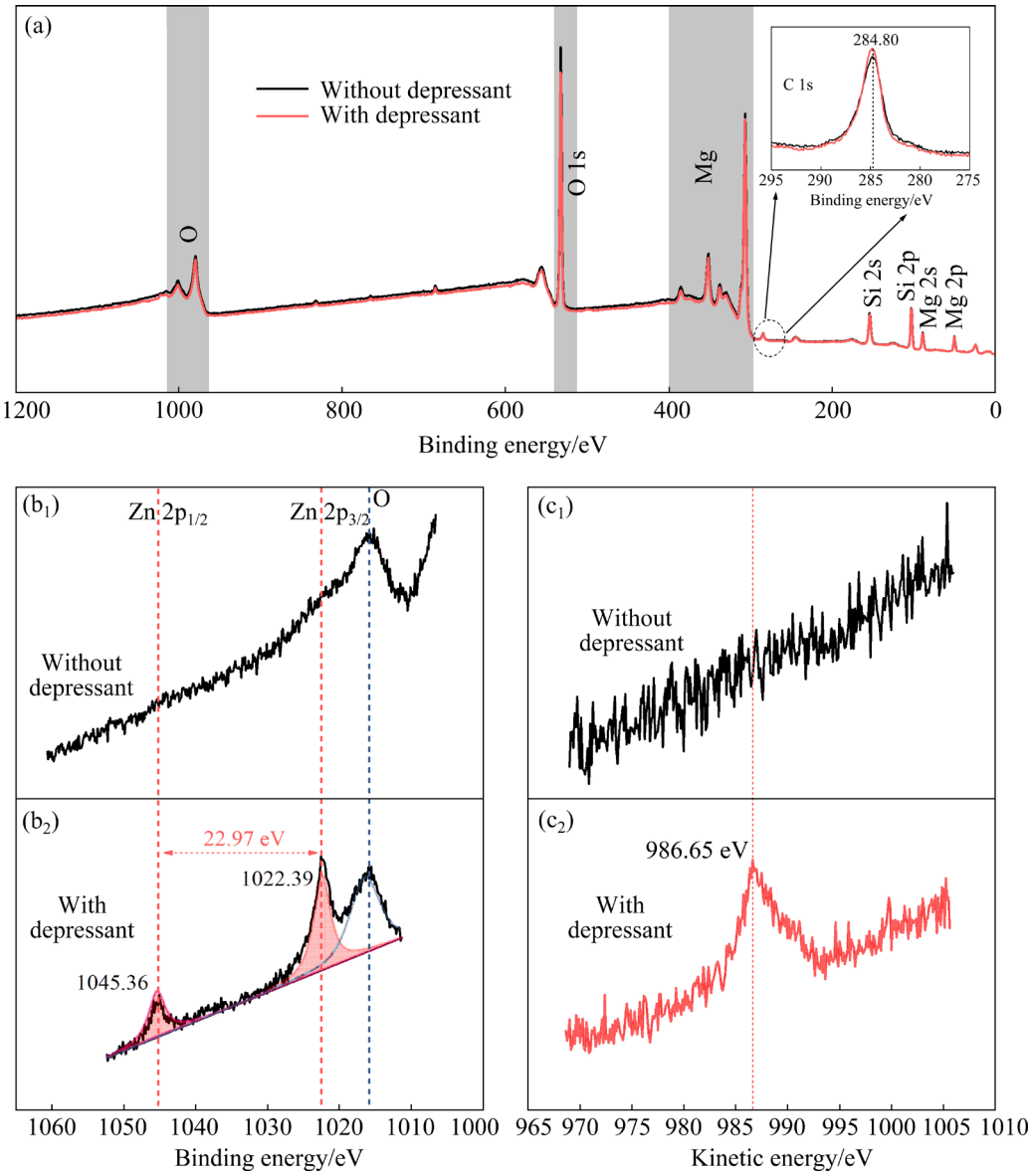

Fig. 9 Survey spectra and high-resolution C1s spectra ((inset in Fig. 9(a)) (a), high-resolution Zn 2p spectra (b_1, b_2), and Zn LMM Auger spectra of talc (c_1, c_2) without and with depressants

The XPS result confirmed the formation of the zinc-bearing precipitate on the talc surface after treatment with the mixed solution of $ZnSO_4$ and Na_2CO_3. Interestingly, both the Zn 2p binding energy and Zn LMM kinetic energy measured from the treated talc surface are close to those previously reported for $Zn_5(CO_3)_2(OH)_6$ [30].

3.6 Surface morphology of talc treated by $ZnSO_4$ and Na_2CO_3

The surface morphology for the talc particles treated with the mixed solutions of $ZnSO_4$ and Na_2CO_3 was imaged in secondary and backscattered electron modes. As shown in the FESEM secondary electron image (Fig. 10(a)), the talc particle has a typical layered structure, and the particle surface is very rough. It can be sure after a careful observation that the morphology of the marked area was different from that of the background area. The corresponding EDS results (Fig. 11) show the marked area with a higher zinc-to-magnesium ratio than the background area. Figure 10(b) presents a backscattered electron image where the zinc-bearing precipitate (the marked area) on the talc surfaces can be seen clearly because of the chemical composition contrast. The FESEM-EDS results further confirmed that the zinc-bearing precipitate was formed on the talc surface.

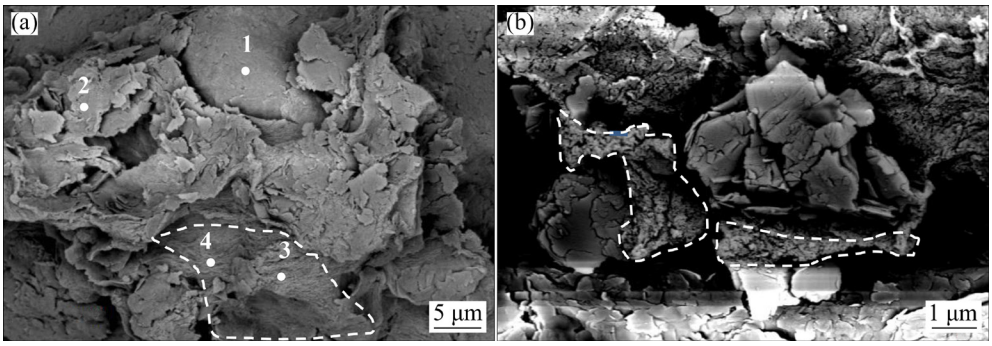

Fig. 10 FESEM secondary electron image (a) and backscattered electron image (b) of talc treated with $ZnSO_4$ and Na_2CO_3 solutions

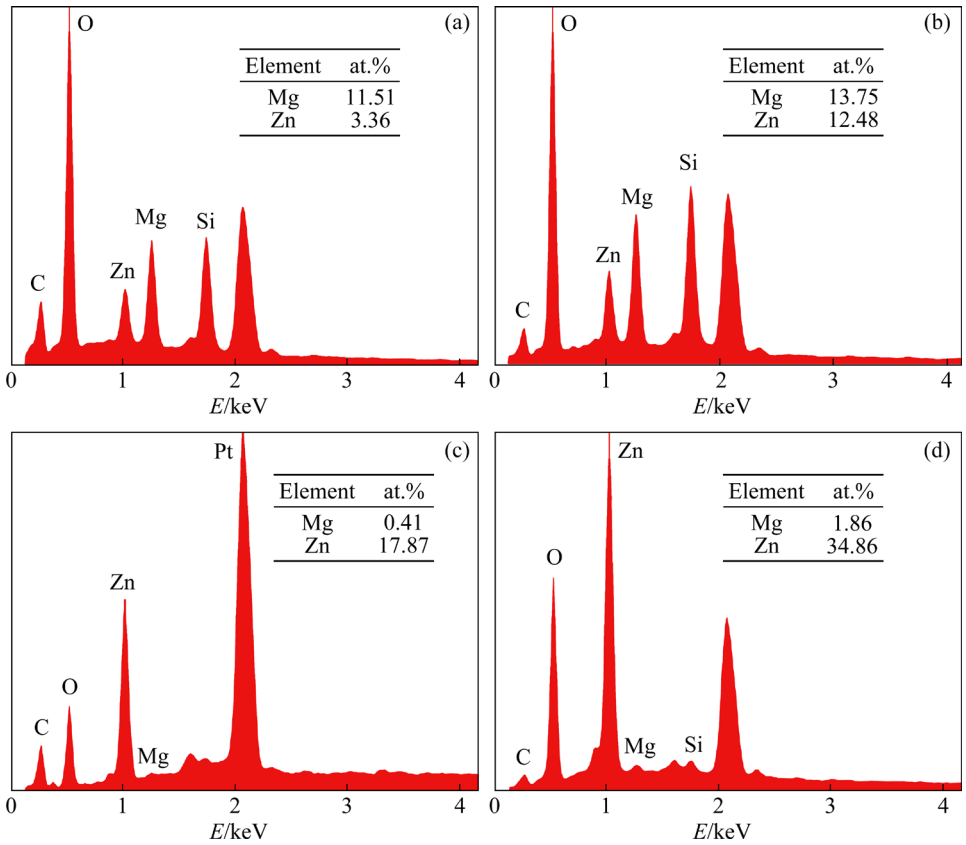

Fig. 11 EDS spectra (a–d) corresponding to spots 1−4 of Fig. 10(a), respectively

3.7 Depression mechanism

Herein, information from the flotation tests, speciation calculations, and characterizations is integrated to elucidate the depression mechanism of the combination of $ZnSO_4$ and Na_2CO_3 on talc flotation.

The flotation tests indicate that the effective depression of talc flotation occurs in the pH range of 7−9. In the pH range, the speciation calculations show that $Zn_5(OH)_6(CO_3)_2$ precipitate is the predominant zinc-bearing specie, which is consistent with the XRD and IR results. In general, colloidal particles with zeta potential values of ±20 mV are unstable and tend to coagulate [31−33]. As a result, both the heterocoagulation of the formed $Zn_5(OH)_6(CO_3)_2$ colloidal particles with other particles and the homocoagulation of the formed $Zn_5(OH)_6(CO_3)_2$ colloidal particles will occur. According to the results of zeta potential measurement, in the pH range of 7−9, the $Zn_5(OH)_6(CO_3)_2$ precipitate is positively charged while the talc surface is negatively charged.

Therefore, strong electrostatic attraction between the formed $Zn_5(OH)_6(CO_3)_2$ colloidal particles and talc appears, and the heterocoagulation of the formed hydrophilic $Zn_5(CO_3)_2(OH)_6$ precipitate with talc will occur predominantly in comparison with the homocoagulation [34]. The XPS and FESEM results confirm that heterocoagulation can indeed occur.

At pH below the precipitation pH of $Zn_5(OH)_6(CO_3)_2$, the dissolved Zn^{2+} ions are the predominant zinc-bearing species, resulting in that talc is not depressed. At high pH, either $Zn_5(OH)_6(CO_3)_2$ or ZnO is the predominant zinc-bearing species. The zeta potential measurement in the present work shows that the PZC of $Zn_5(OH)_6(CO_3)_2$ is at pH 9.4; in addition, previous works suggest that the PZC range of ZnO is from 8.7 to 9.5 [35]. As a result, at pH above 9.5, the zinc-bearing precipitates ($Zn_5(OH)_6(CO_3)_2$ or ZnO) and the talc surface are negatively charged. That is, heterocoagulation is unlikely to occur because of electrostatic repulsion, which is responsible for the absence of talc depression.

In conclusion, the two most crucial questions that must be answered before gaining a deeper understanding of the depression mechanism have been addressed. The findings of this work suggest that the depression of talc flotation is attributed to the heterocoagulation of the formed $Zn_5(OH)_6(CO_3)_2$ precipitate and talc particle mainly due to electrostatic attraction. Based on the results and discussion, a schematic diagram (Fig. 12) elucidates the flotation behavior and depression mechanism of the combination of $ZnSO_4$ and Na_2CO_3 for talc flotation in different pH ranges. However, this work has not been able to provide the reasons for the high selectivity of the $ZnSO_4$–Na_2CO_3 combined depressants. As documented, both chalcopyrite and molybdenite also have a negative surface charge in the pH range where talc flotation was depressed by the combination of $ZnSO_4$ and Na_2CO_3 [36−38]; however, these two sulfide minerals were not significantly depressed. Hence, the mechanism behind the selectivity of the depressants needs further study in the future.

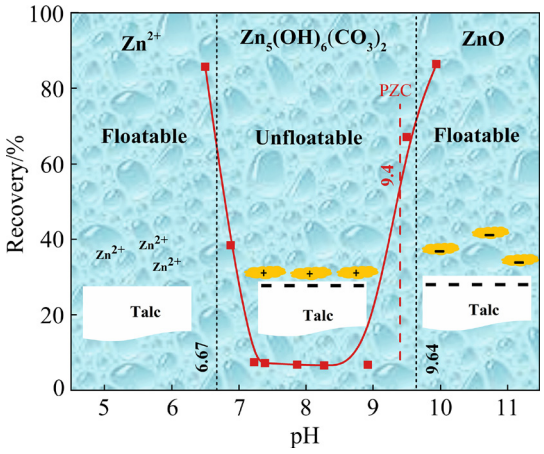

Fig. 12 Schematic illustration of flotation behavior and depression mechanism of talc using combination of $ZnSO_4$ (1 mmol/L) and Na_2CO_3 (1 mmol/L) as depressants in different pH ranges (Talc is shown in white while the zinc-bearing precipitates are shown in yellow)

4 Conclusions

(1) The combination of $ZnSO_4$ and Na_2CO_3 is an effective depressant for talc during flotation of chalcopyrite and molybdenite using xanthate and kerosene as collectors, respectively. However, this depression performance is highly dependent on pulp pH.

(2) In the pH range where the talc depression occurred, $Zn_5(OH)_6(CO_3)_2$ precipitate is the predominant zinc-bearing species; the hetero-coagulation between the positively charged hydrophilic $Zn_5(OH)_6(CO_3)_2$ precipitate and the negatively charged talc particle occurs, primarily due to the electrostatic attraction, thereby resulting in the depression of talc.

(3) Based on this work, when using this combination of depressants, pulp pH should be controlled within the range of 7−9. In practice, adjusting the concentration ratio of Na_2CO_3 to $ZnSO_4$ may be a feasible method of pH adjustment.

Acknowledgments

This research project was supported by the National Natural Science Foundation of China (No. 52074138), the Fundamental Research Project of Yunnan Province, China (No. 202001AS070030), and the Analysis and Testing Foundation of Kunming University of Science and Technology, China (No. 2018M20162101102).

References

[1] YUAN Duo-wei, CADIEN K, LIU Qi, ZENG Hong-bo. Separation of talc and molybdenite: Challenges and opportunities [J]. Minerals Engineering, 2019, 143: 105923.

[2] RAO Shuai, LIU Zhi-qiang, QIU Xian-yang, WANG Dong-xing, CAO Hong-yang, LI Wei, TAO Jin-zhang. Oxygen pressure leaching–flotation joint process for Jinbaoshan platinum group minerals [J]. Transactions of Nonferrous Metals Society of China, 2019, 29(5): 1090−1098.

[3] BEATTIE D A, HUYNH L, KAGGWA G B N, RALSTON J. The effect of polysaccharides and polyacrylamides on the depression of talc and the flotation of sulphide minerals [J]. Minerals Engineering, 2006, 19(6/7/8): 598−608.

[4] JIN Sai-zheng, SHI Qing, LI QI, OU Le-ming, OUYANG Kai. Effect of calcium ionic concentrations on the adsorption of carboxymethyl cellulose onto talc surface: Flotation, adsorption and AFM imaging study [J]. Powder Technology, 2018, 331: 155−161.

[5] CUI Fu-hui, MU Wen-ning, ZHAI Yu-chun, GUO Xue-yi. The selective chlorination of nickel and copper from low-grade nickel-copper sulfide-oxide ore: Mechanism and kinetics [J]. Separation and Purification Technology, 2020, 239: 116577.

[6] NING Shuai, LI Guang-li, SHEN Pei-lun, ZHANG Xiao-lin, LI Jia-lei, LIU Rui-zeng, LIU Dian-wen. Selective separation of chalcopyrite and talc using pullulan as a new depressant [J]. Colloids and Surfaces A: Physicochemical and Engineering Aspects, 2021, 623(1): 126764.

[7] SHORTRIDGE P G, HARRIS P J, BRADSHAW D J, KOOPAL L K. The effect of chemical composition and molecular weight of polysaccharide depressants on the flotation of talc [J]. International Journal of Mineral Processing, 2000, 59(3): 215−224.

[8] RATH R K, SUBRAMANIAN S, LASKOWSKI J S. Adsorption of dextrin and guar gum onto talc: A comparative study [J]. Langmuir, 1997, 13, 23: 6260−6266.

[9] PAN Guang-jiu, SHI Qing, ZHANG Guo-fan, HUANG Gang-hong. Selective depression of talc in chalcopyrite flotation by xanthan gum: Flotation response and adsorption mechanism [J]. Colloids and Surfaces A: Physicochemical and Engineering Aspects, 2020, 600: 124902.

[10] ZHOU Hao, ZHANG Zheng-jun, OU Lei-ming, MAI Qiong-yin. Flotation separation of chalcopyrite from talc using a new depressant carrageenan [J]. Colloids and Surfaces A: Physicochemical and Engineering Aspects, 2020, 603: 125274.

[11] GUO Wei, FENG Bo, PENG Jin-xiu, ZHANG Wen-pu, ZHU Xian-wen. Depressant behavior of tragacanth gum and its role in the flotation separation of chalcopyrite from talc [J]. Journal of Materials Research and Technology, 2019, 8(1): 697−702.

[12] ZHONG Chun-hui, FENG Bo, CHEN Yuan-gan, GUO Meng-chi, WANG Hui-hui. Flotation separation of molybdenite and talc using tragacanth gum as depressant and potassium butyl xanthate as collector [J]. Transactions of Nonferrous Metals Society of China, 2021, 31(12): 3879−3890.

[13] FUERSTENAU M C, LOPEZ-VALDIVIESO A, FUERSTENAU D W. Role of hydrolyzed cations in the natural hydrophobicity of talc [J]. International Journal of Mineral Processing, 1988, 23(3/4): 161−170.

[14] HUCH R O, VALLES P. Talc-molybdenite separation: US, 3921810 [P]. 1975−11−25.

[15] WANG Xing-jie, LIU Rui-zeng, MA Li-yuan, QIN Wen-qing, JIAO Feng. Depression mechanism of the zinc sulfate and sodium carbonate combined inhibitor on talc [J]. Colloids and Surfaces A: Physicochemical and Engineering Aspects, 2016, 501: 92−97.

[16] GUAN You-gou, MING Ping-tian, XIE Zhuo-hong, LI Fei, XING Qing-qing, WANG Zhen. Colloidal $ZnCO_3$ as a powerful depressant of arsenopyrite in weakly alkaline pulp and the interaction mechanism [J]. Minerals, 2020, 10(4): 315.

[17] BAO Yun, XU Guo-qing, TIAN Xiao-dong, MA Jian-tai. Effect of ammonia molecules on the separation of pentlandite from serpentine using copper (II) as activator [J]. Separation and Purification Technology, 2018, 200: 242−254.

[18] LI Wang-qing, LI Yu-biao. Improved understanding of chalcopyrite flotation in seawater using sodium hexametaphosphate [J]. Minerals Engineering, 2019, 134: 269−274.

[19] CUI Yan-fang, JIAO Fen, WEI Qian, WANG Xu, DONG Liu-yang. Flotation separation of fluorite from calcite using sulfonated lignite as depressant [J]. Separation and Purification Technology, 2020, 242(7): 116698.

[20] PAN Zhu-chao, WANG Yun-fan, WEI Qian, CHEN Xin-tao, JIAO Fen, QIN Wen-qing. Effect of sodium pyrophosphate on the flotation separation of calcite from apatite [J]. Separation and Purification Technology, 2020, 242: 116408.

[21] CHENG Jia-qi, PODUSKA K M. A strategy for hydroxide exclusion in nanocrystalline solid-state metathesis products [J]. Nanomaterials, 2013, 3(3): 317−324.

[22] JAMBOR J L. Studies of basic copper and zinc carbonates, Part 1: Synthetic zinc carbonates and their relationship to hydrozincite [J]. Canadian Mineralogist, 1964, 8: 92−108.

[23] ALWAN A K, WILLIAMS P A. Mineral formation from aqueous solution, Part I: The deposition of hydrozincite, $Zn_5(OH)_6(CO_3)_2$, from natural waters [J]. Transition Metal Chemistry, 1979, 4(2): 128−132.

[24] LI Jia-lei, LIU Si-yan, LIU Dian-wen, LIU Rui-zeng, LIU Zhi-cheng, JIA Xiao-dong, CHANG Tian-cang. Sulfidization mechanism in the flotation of cerussite: A heterogeneous solid−liquid reaction that yields $PbCO_3$/PbS core−shell particles [J]. Minerals Engineering, 2020, 153: 106400.

[25] LIU Rui-zeng, LIU Dian-wen, LI Jia-lei, LI Jian-ming, LIU Zhi-cheng, JIA Xiao-dong, YANG Sheng-wang, LI Jiang-li. Sulfidization mechanism in malachite flotation: A heterogeneous solid-liquid reaction that yields Cu_xS_y phases grown on malachite [J]. Minerals Engineering, 2020, 154: 106420.

[26] BUCCA M, DIETZEL M, TANG Jian-wu, LEIS A L, KÖHLER S J. Nucleation and crystallization of otavite, witherite, calcite, strontianite, hydrozincite, and hydrocerussite by CO_2 membrane diffusion technique [J]. Chemical Geology, 2009, 266(3/4): 143−156.

[27] HALE M C, FROST R L. Synthesis and vibrational spectroscopic characterization of synthetic hydrozincite and smithsonite [J]. Polyhedron, 2007, 26(17): 4955−4962.

[28] STOILOVA D, KOLEVA V, VASSILEVA V. Infrared study of some synthetic phases of malachite ($Cu_2(OH)_2CO_3$)–hydrozincite ($Zn_5(OH)_6(CO_3)_2$) series [J]. Spectrochimica

Acta Part A: Molecular and Biomolecular Spectroscopy, 2002, 58: 2051−2059.

[29] LIU Rui-zeng, PEI Bin, LIU Zhi-cheng, WANG Yun-wei, LI Jia-lei, LIU Dian-wen. Improved understanding of the sulfidization mechanism in amine flotation of smithsonite: An XPS, AFM and UV−vis DRS study [J]. Minerals, 2020, 10(4): 370.

[30] DAKE L S, BAER D R, ZACHARA J M. Auger parameter measurements of zinc compounds relevant to zinc transport in the environment [J]. Surface and Interface Analysis, 1989, 14: 71−75.

[31] SALAZAR-BRYAM A M, YOSHIMURA I, SANTOS L P, MOURA C C, SANTOS C C, SILVA V L, LOVAGLIO R B, MARQUES R F C, Jr JAFELICCI M, CONTIERO J. Silver nanoparticles stabilized by ramnolipids: Effect of pH [J]. Colloids and Surfaces B: Biointerfaces, 2021, 205: 111883

[32] BIJARBOONEH F H, ZHAO Yue, KIM J H, KIM J H, SUN Zi-qi, MALGRAS V, ABOUTALEBI S H, HEO Y U, IKEGAMI M, DOU Shi-xue. Aqueous colloidal stability evaluated by zeta potential measurement and resultant TiO_2 for superior photovoltaic performance [J]. Journal of the American Ceramic Society, 2013, 96(8): 2636−2643.

[33] POCHAPSKI D J, SANTOS C C D, LEITE G W, PULCINELLI S H, SANTILLI C V. Zeta potential and colloidal stability predictions for inorganic nanoparticle dispersions: Effects of experimental conditions and electrokinetic models on the interpretation of results [J]. Langmuir, 2021, 37(45): 13379−13389.

[34] FURUSAWA K, ANZAI C K. Heterocoagulation behaviour of polymer latices with spherical silica [J]. Colloids & Surfaces, 1992, 63(1/2): 103−111.

[35] FATEHAH M O, AZIZ H A, STOLL S. Stability of ZnO nanoparticles in solution. influence of pH, dissolution, aggregation and disaggregation effects [J]. Journal of Colloid Science & Biotechnology, 2014, 3(1): 75−84.

[36] WEI Qian, JIAO Fen, DONG Liu-yang, LIU Xue-duan, QIN Wen-qing. Selective depression of copper-activated sphalerite by polyaspartic acid during chalcopyrite flotation [J]. Transactions of Nonferrous Metals Society of China, 2021, 31: 1784−1795.

[37] KHOSO S A, HU Yue-hua, LÜ Fei, GAO Ya, LIU Run-qing, SUN Wei, Xanthate interaction and flotation separation of H_2O_2-treated chalcopyrite and pyrite [J]. Transactions of Nonferrous Metals Society of China, 2019, 29: 2604−2614.

[38] PENG Ying, LI Yu-biao, LI Wan-qing, FANG Xin, LIU Cheng, FAN Rong. Elimination of adverse effects of seawater on molybdenite flotation using sodium silicate [J]. Minerals Engineering, 2020, 146: 106108.

硫酸锌和碳酸钠抑制滑石浮选机理

李佳磊[1]，马印禹[2]，李广利[3]，刘志成[3]，宁 帅[1,4]，裴 斌[1]，郎召有[3]，刘瑞增[1,4]，刘殿文[1,4]

1. 昆明理工大学 国土资源工程学院，昆明 650093；
2. 锡林郭勒盟山金阿尔哈达矿业有限公司，锡林郭勒 026300；
3. 云南驰宏锌锗股份有限公司，曲靖 655000；
4. 云南省战略金属矿产资源绿色分离与富集重点实验室，昆明 650093

摘 要：通过浮选试验、溶液化学计算和多种表征技术，深入研究硫酸锌和碳酸钠在黄铜矿和辉钼矿浮选中对滑石的抑制机理。浮选试验表明，在 pH 值为 7~9 的范围内滑石浮选得到有效抑制。在该 pH 范围内，对硫酸锌和碳酸钠混合溶液的溶液化学计算表明，碱式碳酸锌是主要的含锌物种；X 射线衍射和红外光谱分析进一步证明了这一点。Zeta 电位测试表明：在滑石抑制发生的 pH 范围内，碱式碳酸锌表面带正电荷，而滑石表面带负电荷。X 射线光电子能谱和场发射扫描电子显微镜证实：经硫酸锌和碳酸钠混合溶液处理的滑石颗粒表面存在含锌沉淀物。结果表明，由于静电吸引，形成的碱式碳酸锌与滑石发生异相聚沉，从而抑制滑石浮选。

关键词：滑石；浮选分离；抑制；异相聚沉；静电吸引；碱式碳酸锌

(Edited by Xiang-qun LI)